JOURNAL OF AIRCRAFT
Vol. 31, No. 4, July–Aug. 1994

Experimental Investigation of Rotor/Lifting Surface Interactions

J. G. Leishman*
University of Maryland College Park, College Park, Maryland 20742
and
Nai-Pei Bi†
Advanced Technologies, Inc., Newport News, Virginia 23606

Experiments were conducted to study the aerodynamic interactions between a rotor and a fixed lifting surface. A low aspect ratio rectangular wing was positioned at different locations in a rotor flowfield to simulate the aerodynamic environment encountered by the wings of tilt-rotors or the empennage of helicopters. Steady and unsteady pressure measurements were made on the wing at various chordwise and spanwise stations for different combinations of rotor thrust and advance ratio. Flow visualization was performed using the wide-field shadowgraph method, which helped to identify the locations of the rotor wake relative to the rotor and wing. The results have shown that the lifting surface operates in a highly unsteady three-dimensional flow environment with regions of partial or complete flow separation. In addition, large unsteady loads were induced on the wing by the rotor and its wake.

Nomenclature

C_p^u = time-dependent pressure coefficient, $100[p(t) - p_\infty]/0.5\rho\Omega^2R^2$
C_p' = time-averaged pressure coefficient, $100(p - p_\infty)/0.5\rho\Omega^2R^2$
C_T = rotor thrust coefficient, $T/\rho\pi\Omega^2R^4$
c_b = rotor blade chord, m
c_w = chord of lifting surface, m
k = reduced frequency
N_b = number of rotor blades
p = static pressure, N/m^2
R = rotor radius, m
r = mondimensional rotor radius
T = rotor thrust, N
t = time, s
V_i = time-averaged induced velocity, m/s
V_∞ = freestream velocity, m/s
x, y = wing coordinate system, m
x_h, y_h = rotor coordinate system relative to hub, m
α_s = rotor shaft angle (tip-path-plane angle), deg
μ = advance ratio, $V_\infty/\Omega R$
ρ = air density, kg/m^3
σ = rotor solidity, $N_b c_b/\pi R$
ψ = blade azimuth angle, deg
Ω = rotor rotational speed, rad/s
ω = circular frequency, rad/s

Introduction

RECENT advances in helicopter rotor design have permitted the use of higher disk loadings for a given gross weight. However, higher disk loadings result in higher wake slipstream velocities and stronger tip vortices. In hover and low-speed forward flight, the fuselage and empennage will be immersed inside the boundaries of the rotor wake,[1] and this can produce acute rotor/airframe interactions. The trend toward using reduced rotor/airframe spacings also tends to amplify interactional loads, mainly through unsteady effects, which are manifest as strong blade passage pressure pulses and tip vortex impingement on the airframe. In addition, the effect of the airframe and the associated wake distortions cause a reciprocal effect on the rotor. This results in a change of the induced inflow distribution through the rotor disk, and therefore, a change in rotor loads, vibration levels, and rotor performance.[2] It is clear that aerodynamic interactional effects are becoming an increasingly important consideration in rotorcraft design.

The general field of rotor/airframe interactional aerodynamics has been researched for several years. While there have been earlier contributions to the problem (see Ref. 3 for a recent review), the first systematic study is usually attributed to Sheridan and Smith.[4] This work has led to general design guidelines to minimize the problems associated with rotor/body and rotor/empennage interactions on helicopters. However, the aerodynamic mechanisms responsible for these interactions are still not fully understood. In recent years, a significant amount of detailed experimental and theoretical research has been accomplished to provide a more thorough physical understanding of the aerodynamic interactions between rotors and (nominally) nonlifting bodies (see, e.g., Refs. 5–13). There has been particular experimental and theoretical emphasis on the transient airloads caused by the interaction of discrete rotor tip vortices with the airframe surfaces.[1,14] However, vortex impingement phenomena are very localized on the airframe surface and contributes more to airframe vibrations than to the net aerodynamic loads.

The interactions between rotors and lifting surfaces, such as those comprising the empennage of helicopters and tilt-rotors, are known to be particularly significant, yet systematic studies of the problem still remain relatively few. Lynn[15] has discussed some of the general problems associated with helicopter rotor/wing interactions, concentrating mostly on performance issues. Historically, empennage designs on helicopters have proved problematic, mainly from a stability and control perspective. Under some circumstances, especially during the transition from hover to forward flight, the helicopter tailplane may operate intermittently inside the rotor

Presented as Paper 93-0871 at the AIAA 31st Aerospace Sciences Meeting and Exhibit, Reno, NV, Jan. 11–14, 1993; received Jan. 31, 1993; revision received Aug. 18, 1993; accepted for publication Sept. 3, 1993.

*Associate Professor, Department of Aerospace Engineering. Senior Member AIAA.
†Engineering Specialist. Member AIAA.

wake boundary. This situation can produce an aircraft with very undesirable handling qualities; the difficulties with the prototype AH-64 and EH-101 helicopters are documented examples of this problem.[16,17]

While rotor/tailplane interactions have proved to be significant on helicopters, rotor/wing and rotor/empennage interactions are particularly acute on tilt-rotor aircraft. In hover (helicopter mode), the main wings are directly below the rotors and immersed in the rotor wakes. In forward flight (airplane mode), both the main wings and the tail surfaces can be located inside the rotor wake boundaries. Under these conditions, the interactions between the rotor wake vortices and the empennage are known to constitute a significant source of vibratory loads, hence the significant work on tilt-rotor aerodynamic interactions.[18-21]

The theoretical prediction of the effects of rotors and the associated vortical wakes on the airloads induced on wings and bodies has received considerable attention. Bramwell[22] was one of the first to use potential flow methods to examine this problem, and the significance of unsteady effects was clearly demonstrated at that time. However, the development of more sophisticated analytical methods has been hindered by the lack of detailed experimental data for guidance in developing the models themselves, and particularly for validation purposes. Gangwani[23,24] used a prescribed wake model coupled with a doublet-lattice model of a fixed wing to predict the unsteady bending moments measured on a helicopter stabilator. Reasonable correlation was obtained. Mello and Rand[25] used a similar model, and showed that the predicted unsteady loads were very sensitive to the rotor wake geometry. Curtiss and Quackenbush[26] considered the effects of the rotor wake induced velocity field at the empennage location on helicopter stability derivatives. The limited correlations obtained with flight test data reiterated the complexity of the wake/empennage interaction problem. Recently, Weinstock[27] has examined a simplified model of the same problem for use in rotor flight mechanics.

An improved understanding of the rotor/lifting surface interaction problem presents several experimental and theoretical challenges to the analyst. In addition to the high rotor downwash at the empennage, there are several possible constituent sources of unsteady loading that may be produced on a lifting surface located near a rotor. It is known that for the nonlifting (body) case, unsteady effects induced by the rotor and its wake can be extremely large.[1] One unsteady effect is due to blade passage, which produces an impulsive type of noncirculatory loading on the surface. Another is due to the presence of the rotor tip vortices, which induce rapid changes in downwash and produce both noncirculatory and circulatory aerodynamic loads. In addition to the rotor effects, there may be time-dependent aerodynamic effects due to the trailed and shed wake generated by the lifting surface(s). The relative magnitude of all these effects will depend on the proximity of the lifting surface to the rotor, the wake slipstream velocity, the tip vortex strengths, and the proximity of the wake to the lifting surface. The latter, of course, will be sensitive to the flight condition, i.e., the rotor thrust and advance ratio.

In view of the present limited understanding of these interrelated effects, the purpose of this work was to initiate a systematic experimental investigation into the problem of rotor/lifting surface interactions. Particular emphasis was placed on documenting the unsteady effects. The overall objective was to obtain a better understanding of the aerodynamic environment encountered by lifting surfaces near a rotor and/or immersed in the rotor wake, and to provide some basic measurements for comparison with analytical models. The work also provides a foundation for more detailed studies on the problem.

Description of the Experiment

The experimental setup consisted of a rotor and a generic lifting surface (wing). In most tests, the rotor drive mechanism was covered by a minimum body aerodynamic fairing, and in the remaining tests, a larger body of revolution was used. The rotor had a fully articulated hub with four blades, and conventional swashplate arrangement. The rotor was 1.65 m (65 in.) in diam, and the blades were rectangular in planform with -13 deg of linear twist. Further details of the rotor apparatus are described in Refs. 28–30.

Table 1 Main characteristics of the rotor, fuselage, and lifting surface

N_b	4
R	0.8255 m (32.5 in.)
c_b	0.0635 m (2.5 in.)
σ	0.098
Blade twist (linear)	-13 deg
Taper ratio	1.0
Blade airfoil	NASA RC(3)/(4) series
Body length	1.94 m (76.5 in.)
Body max, diam	0.254 m (10.0 in.)
Wing aspect ratio	2.0
Wing chord c	0.3048 m (12.0 in.)
Wing airfoil	NACA 0014

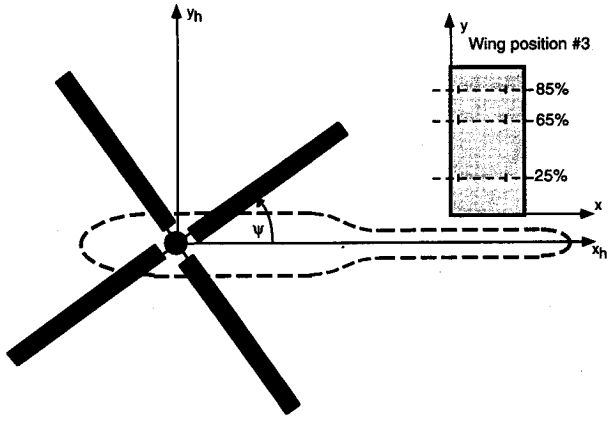

Fig. 1 General arrangement of the rotor, fuselage, and lifting surface in the wind tunnel.

The wing used for the interaction studies had a constant chord of 0.305 m (1 ft), an aspect ratio of 2, and employed an NACA 0014 airfoil. Figure 1 shows the setup in the wind tunnel. The wing was mounted separately in the flowfield on a single support, and was at 0-deg angle of attack relative to the freestream flow. A summary of the main characteristics of the rotor, fuselage, and lifting surface models are given in Table 1.

Instrumentation

Rotor and Wing Instrumentation

Instrumentation was provided on the rotor and the lifting surface. The rotor balance permitted the measurement of three mutually perpendicular time-averaged force components (thrust, drag, and side-force), along with the corresponding moments about these axes. Rotor power was measured using a torque disk coupled to the rotor shaft by means of a flexible diaphragm. Hall-effect sensors were located at the flap and lead/lag hinges to monitor flap and lead/lag displacements, respectively. Details of other rotor instrumentation are given in Ref. 28.

Time-averaged pressures were measured at 29 locations on the lifting surface, at three spanwise stations [30, 60, and 80% span (see Table 2)]. All odd numbered taps were on the upper wing surface. Static pressures were measured using a digital multichannel pressure system. The pressure tubes were connected to a thermally insulated multiplexer module mounted inside the wing. Port connections were made using internal restrictors to ensure that any tubing resonant frequencies were much higher than the fundamental flowfield frequency (4/rev $\approx$ 132 Hz). The pressure measuring module contained min-

Table 2 Locations of static pressure taps on the wing

Tap no.	x/c, %	y/c, %
1	0.0	30.0
2, 3	5.0	30.0
4, 5	11.5	30.0
6, 7	38.5	30.0
8, 9	63.9	30.0
10	0.0	60.0
11, 12	5.0	60.0
13, 14	11.5	60.0
15, 16	38.5	60.0
17, 18	50.0	60.0
19, 20	63.9	60.0
21, 22	76.8	60.0
23	0.0	80.0
24, 25	5.0	80.0
26, 27	11.5	80.0
28, 29	63.9	80.0

Table 3 Locations of dynamic pressure transducers

Sensor no.	x/c, %	y/c, %
1, 2	5.0	25.0
3, 4	11.5	25.0
5, 6	38.5	25.0
7, 8	63.9	25.0
9, 10	76.8	25.0
11, 12	5.0	65.0
13, 14	11.5	65.0
15, 16	38.5	65.0
17, 18	50.0	65.0
19, 20	63.9	65.0
21, 22	76.8	65.0
23, 24	5.0	65.0
25, 26	11.5	65.0
27, 28	38.5	85.0
29, 30	63.9	85.0
31, 32	76.8	85.0

Table 4 Locations wing reference point relative to rotor hub center

Position	x_h/R	y_h/R
1	−0.102	0.215
2	−0.102	−0.954
3	1.237	0.215
4	1.237	−0.954

Table 5 Summary of test parameters

Parameter	Test values
μ	0.05, 0.075, 0.1, 0.125, 0.15, 0.2, 0.25
V_∞	8.6, 12.8, 17.1, 21.4, 25.7, 34.2, 42.8 m/s
α_s	−6 deg
C_T/σ	0.065, 0.075, 0.085
Rotor speed	1980 rpm (33 Hz)
Rotor hover tip Mach no.	0.53

iature quartz pressure transducers, analog multiplexers, and analog-to-digital converters. A miniature pneumatic valving system inside the module permitted rapid on-line recalibration of the pressure sensors with the test in progress. Frequent recalibration was essential to maintain a measurement accuracy of 7.5 Pa (0.0011 lb/in.^{2}) over considerable tunnel run times.

Time-dependent pressures were measured using piezoelectric pressure transducers at 32 locations, and grouped at three spanwise stations [25, 65, and 85% span (see Table 3)], again

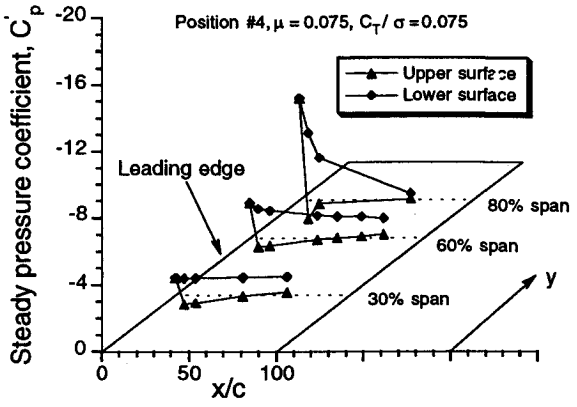

Fig. 2 Time-averaged pressure distribution on the lifting surface for $\mu = 0.075$ and $C_T/\sigma = 0.075$ at aft position no. 4.

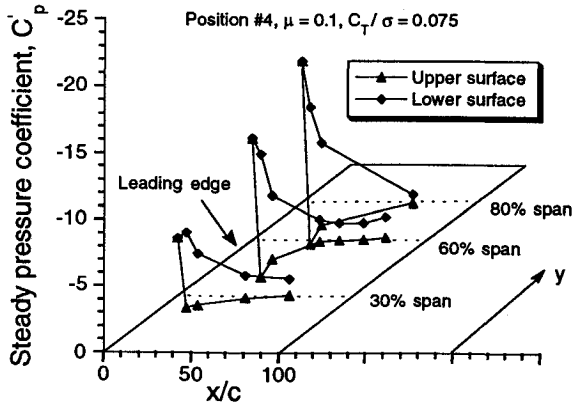

Fig. 3 Time-averaged pressure distribution on the lifting surface for $\mu = 0.10$ and $C_T/\sigma = 0.075$ at aft position no. 4.

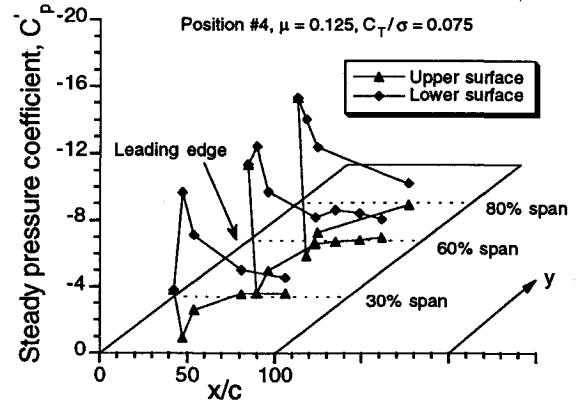

Fig. 4 Time-averaged pressure distribution on the lifting surface for $\mu = 0.125$ and $C_T/\sigma = 0.075$ at position no. 4.

with odd numbered sensors on the upper surface. Due to physical constraints, it was impractical to collocate the pressure transducers at the same chordwise or spanwise locations as the static pressure taps, and they were offset slightly. Based on step response tests, the resonant frequency of the sensors were near 12 kHz, which was well in excess of the frequencies to be measured. A harmonic analysis of the measured unsteady pressure data showed a negligible response for frequencies above 600 Hz, i.e., about 20/rev.

Flow Visualization

The wide-field shadowgraph technique was used to visualize the locations of the strong rotor tip vortices relative to the lifting surface. The basic components of the shadowgraph system are a high intensity point light source strobe, a retroreflective screen, and a video camera. The tip vortices created

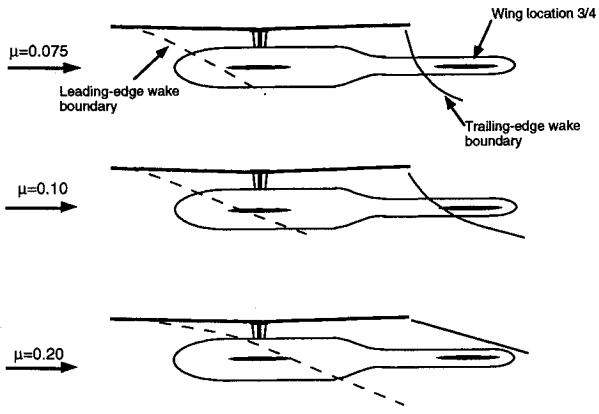

Fig. 5 Measured leading- and trailing-edge rotor wake boundaries in forward flight.

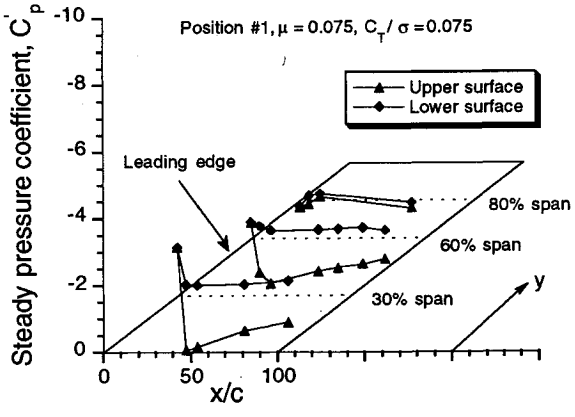

Fig. 6 Time-averaged pressure distribution on the lifting surface for $\mu = 0.075$ and $C_T/\sigma = 0.075$ at forward position no. 1.

by the rotor cause small changes in the flow density. As the light rays from the strobe pass through these vortices they are refracted, and cause shadows of the vortices to be cast on the screen. By examining the wake for successive rotor azimuth positions, and by using a grid system on the screen, it was possible to quantify the locations of the leading and trailing edges of the rotor wake boundary relative to the rotor and the lifting surface. Further details of the wide-field shadowgraph technique as applied in this experiment can be found in Ref. 29.

Data Acquisition System

Data acquisition was controlled by a minicomputer. Time-averaged pressure data were acquired from the pressure measuring system over a digital interface. Quasisteady data, such as rotor balance loads, were logged directly by the computer through a 16-channel multiplexer and a 12-bit analog-to-digital (A/D) converter. Unsteady pressure data were logged using a high-speed multichannel 12-bit A/D converter system. This data acquisition system was also interfaced with the computer over a digital interface. Triggering was synchronized to a 1/rev pulse initiated from an encoder on the rotor shaft.

The steady or time-averaged pressure measurements were made over a 3-s time interval corresponding to 99 rotor revolutions. Time histories of the pressure transducer responses were logged continuously over 10 revolutions at a sampling resolution of 256 data frames per channel per rotor revolution, i.e., an azimuth resolution of 1.4 deg. All of the unsteady data presented in this article are event-averaged, i.e., the data were first ensemble-averaged over 10 rotor revolutions, and since a four-bladed rotor was used, the results were further ensemble-averaged over 90 deg of blade azimuth angle. The estimated error in C_p' was ± 0.01. The maximum likely estimated error in C_p^u was about ± 0.05.

Test Conditions

The experiments were performed in the University of Maryland's Glenn L. Martin closed-return wind tunnel, which has a 2.36- × 3.35-m (8- × 11-ft) working section. The rotor was tested at a rotational speed of 1980 rpm (33 Hz), which corresponded to a nominal tip Mach number of 0.50 and a tip Reynolds number of 7.44×10^5 in hover. Collective, lateral cyclic, and longitudinal cyclic blade pitch were set remotely by means of swashplate actuators. The trim procedure was performed by minimizing the 1/rev blade flapping response relative to the shaft, which ensured that the rotor tip-path plane (TPP) was perpendicular to the rotor shaft axis.

The lifting surface was positioned at four different horizontal locations, and several vertical heights relative to the rotor; the location of the wing reference point (port tip leading edge) relative to the hub for the four positions are given in Table 4, see also Fig. 1. In this article, data are discussed for the highest wing position, which was 23.62 cm (9.3 in.) or $0.286\%R$ below the rotor hub plane. These wing positions roughly simulated the conditions likely to be encountered by the main wing of a tilt-rotor configuration (or stub wing on a helicopter), as well as a horizontal stabilizer on a helicopter or tilt-rotor.

Over 100 test conditions comprising variations in rotor thrust and advance ratio were examined; the range test parameters are summarized in Table 5. Tests were conducted both with and without the fuselage (body) in the flowfield, although in most cases the effects of the fuselage were found to be minor and are not discussed in this article. When the fuselage was removed, the rotor drive mechanism was covered by a minimum body fairing.[30] Comparative studies were conducted at a constant rotor thrust. For brevity, only selected results can be shown in this article, with all data being for a blade loading coefficient C_T/σ of 0.075. Also, a single rotor TPP angle of -6 deg (forward shaft tilt) was examined, since it was found that the loads on the wing were relatively insensitive to TPP angle of attack. Note that due to this tilt of the TPP, the wing was at a positive 6-deg angle of attack relative to the TPP.

Results and Discussion

Time-Averaged Airloads

Time-averaged pressure distributions on the lifting surface were measured on both the upper and lower surfaces at three spanwise stations, as given in Table 2. These measurements were used to help interpret the state of the flow on the wing, i.e., whether it was attached, partially separated, or fully separated.

Lifting Surface in Aft Position

Typical chordwise pressure coefficient distributions measured on the lifting surface when positioned at the aft position (tailplane location) are shown in Fig. 2. Similar results were obtained for both the retreating and advancing sides, and so for this article the results are presented only for position no. 4, which is on the retreating (left) side of the rotor disk. In this case, the wing 80% span station is further inboard and closer to the longitudinal centerline of the rotor.

From Fig. 2, it can be seen that only the inboard section of the lifting surface exhibits a chordwise pressure distribution symptomatic of attached flow, with high suction pressures on the lower surface near the leading edge. At the outboard sections, the uniform pressure distribution on the lower surface suggests that the flow is separated. From these measurements, it can be inferred that all three sections of the wing surface were operating at large negative effective angles of attack, but with the largest angles of attack biased toward the outboard parts of the wing. These large negative angles of attack are a result of the high local downwash created by the rotor at $\mu = 0.075$.

As the advance ratio was increased from 0.075 to 0.10, as shown in Fig. 3, all three spanwise stations now showed chord-

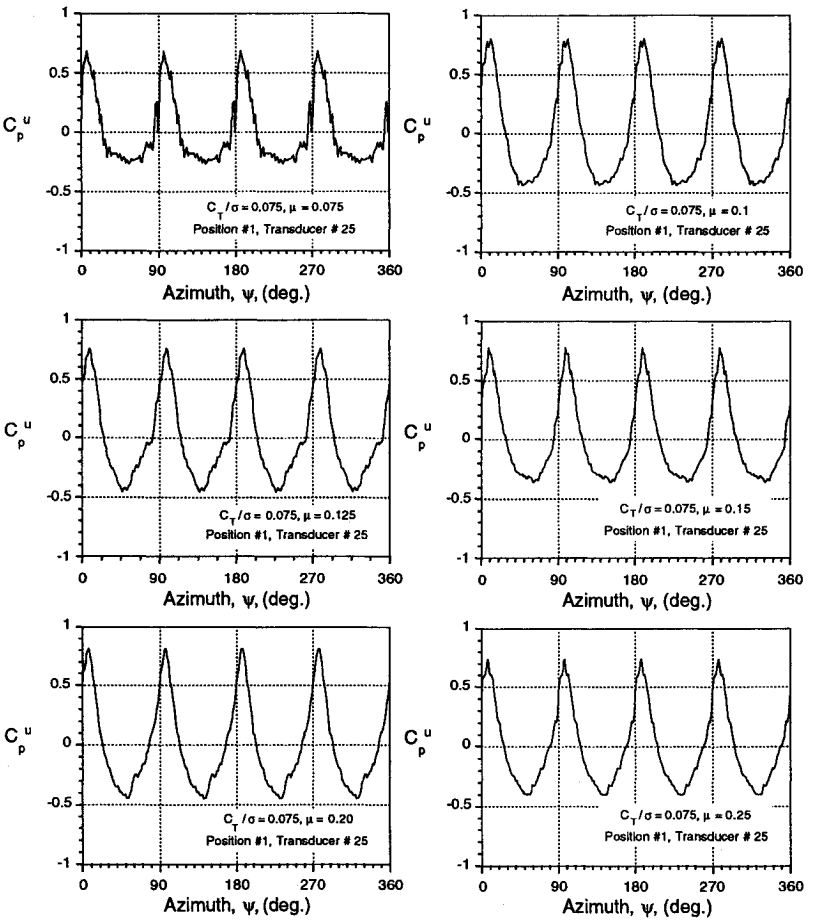

Fig. 7 Unsteady pressures measured on outboard part of lifting surface at forward position no. 1 for several advance ratios, $C_T/\sigma = 0.075$.

wise pressure distributions that were symptomatic of either fully or partially attached flow. Much larger suction pressures were created at the leading edge of the lower surface at all three stations. Thus, it was clear that the flow had begun to reattach to the surface as the advance ratio was increased over this range. This was mainly due to the decrease in the induced flow angle at the wing location (or increase in wake skew angle) as the advance ratio was increased. However, it can be seen from Fig. 3 that there is still a highly nonuniform flow over the lifting surface, with the inboard section producing the largest amount of negative lift. At the outboard spanwise stations, only partially attached flow occurred on the surface. This is especially the case at the 60% span locations, where there is evidence of significant trailing-edge separation.

As the advance ratio was increased from 0.10 to 0.125 and higher, it was found that the whole lifting surface operated with nominally attached flow, as typified by Fig. 4. At this advance ratio the rotor wake skew angle was found to be much larger with lower downwash velocities and higher streamwise velocities,[30] and so the induced flow angles of attack at the wing are correspondingly much smaller. However, some evidence of separation can still be seen at the 60% span location. By means of wake surveys and flow visualization, for the conditions given in Fig. 4 the local wake skew angle was found to be close to 75 deg, giving an average aerodynamic angle of attack at the lifting surface of about −15 deg. In fact, for $\mu = 0.125$, it can be seen from Fig. 4 that the outboard sections are now operating at high negative lift conditions, just below the stall. As the advance ratio was increased further, the flow separation further inboard became less in extent due to the higher local skew angle of the wake, reducing the local angles of attack (and lift) at the wing location.

Figure 5 shows a summary of the measured boundaries of the leading and trailing edges of the wake relative to the rotor and the lifting surface positions. These boundaries were defined using flow visualization and velocity field measurements. At the front of the disk, the tip vortices are initially convected above the rotor, and then pass through the rotor downstream of the leading edge of the disk. These interactions with the blades tend to break up the structure of the tip vortices, and the wake boundary could be defined only by means of the flow survey. At the rear of the wake the tip vortex filaments remained intact for a considerable wake age, and were easily observed by means of the shadowgraph method.

Lifting Surface in Forward Position

Figure 6 shows the time-averaged pressure measured at position no. 1 (advancing side) for an advance ratio of 0.075. The flow at the 80% spanwise station (that is now the most outboard station) is completely separated over the lower surface. Again, this indicates that this portion of the wing was operating at very high (negative) effective angles of attack. The 60 and 30% spanwise stations also show evidence of significant flow separation. At this forward wing location, the rotor produces a somewhat lower induced downwash, and therefore a higher local skew angle and lower induced angles of attack are produced. However, there is also a significant lateral variation in downwash, giving an induced angle-of-attack distribution that is biased toward the outboard regions of the rotor disk.[30] In general, the trends noted when the wing was in the aft position were also noted here. That is, with increasing advance ratio at a constant thrust, the flow was found to reattach to the wing. Conversely, with increasing thrust at a constant advance ratio, the flow becomes more highly separated on the lower surface of the wing.

Time-Dependent Airloads

An examination of the time-dependent pressures on the lifting surface was another goal of the present work. These

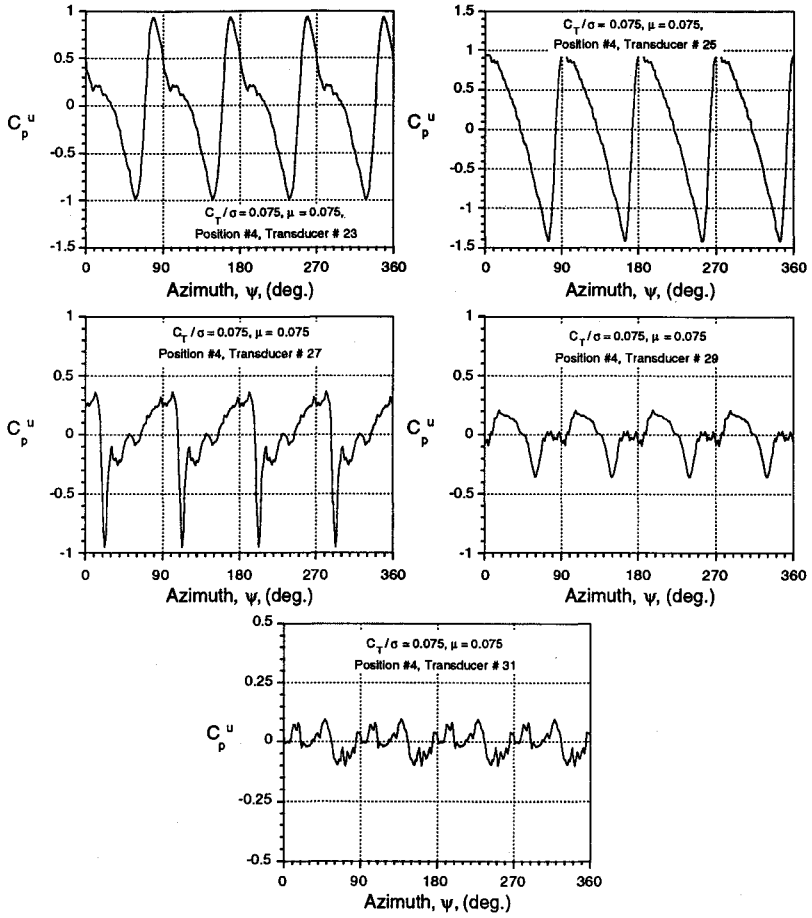

Fig. 8 Typical unsteady pressures measured on lifting surface at position no. 4, $C_T/\sigma = 0.075$.

measurements were converted to coefficient form as values of $C_p'(t)$, and are presented in terms of the alternating component only. The time-scale is based on the blade azimuth angle, with time zero being measured when the ¼-chord of the reference blade was pointing in the downstream direction ($\psi = 0$ deg).

A spectral analysis of the unsteady pressure measurements showed that the dominant frequency at nearly every location was at 4 per rotor revolution $4P$, although many locations showed significant responses at $8P$, $12P$, and $16P$. Of course, the fundamental source of these loads is the rotor, but there are several possible constituent sources of unsteady loading. For locations near to the rotor, blade passage effects produce a strong impulsive type of noncirculatory loading on the surface. At other locations, the rotor tip vortices will induce rapid changes in angle of attack as they are convected near the wing, and therefore, time-dependent aerodynamic loads will be produced. There may also be time-dependent aerodynamic effects due to the trailed and shed wake generated by the wing itself. Clearly, the relative magnitude of all these effects will depend on several interrelated parameters, and the purpose of this part of the experiment was to gain some insight into the problem.

Lifting Surface at Forward Position

Figure 7 shows the time-dependent pressure coefficients measured at location no. 25 (85% span station, $x/c = 11.5\%$) on the upper surface for several advance ratios from 0.075 to 0.25. The lifting surface was located on the advancing side of the rotor in this forward position, although very similar results were obtained for the opposite (retreating) side. It can be seen from Fig. 7 that for all advance ratios the unsteady pressure signature is of a characteristic blade passage-type, which consists of four strong pressure pulses per rotor revolution. A detailed discussion of the pressure signatures induced by blade passage can be found in Refs. 22 and 31.

For stations further inboard on the wing and closer to the rotational axis of the rotor (not shown) the induced pressure signatures were found to be very similar, again with four large pulses per rotor revolution, although the magnitude of the fluctuations were found to be somewhat lower. Small, but significant, phase differences in the pressure peaks were also found to exist for inboard measurement locations. These phase differences arise because the blade passes over the transducers at different times or azimuthal angles. In addition, it was noted the magnitude of the signature became somewhat smaller toward the trailing edge of the lifting surface, and the pressure responses showed evidence of more complicated loads at $4P$ and $8P$.

While significant time-dependent pressure pulses were measured at nearly all points on the upper surface of the wing at the forward locations, much less definite pressure signatures were observed on the lower surface (not shown). The net effect is large fluctuating ($4P$) and nonzero time-averaged noncirculatory lift forces on the wing, as well as a $4P$ pitching moment because the pressure pulse is felt at different chordwise positions at different azimuthal times.

Lifting Surface at Aft Position

Unlike the time-dependent pressures measured at the forward position, the pressure signatures measured on the lifting surface at positions 3 and 4 showed many more complex variations. At the aft wing locations, the unsteady loads are closely related to the proximity of the rotor tip vortices. Figure 8 shows representative time-dependent pressures measured at wing position no. 4 for five chordwise locations on the upper surface at the 85% span station, i.e., the station closest to the longitudinal centerline of the rotor. Note that the pressure responses vary from fairly large near

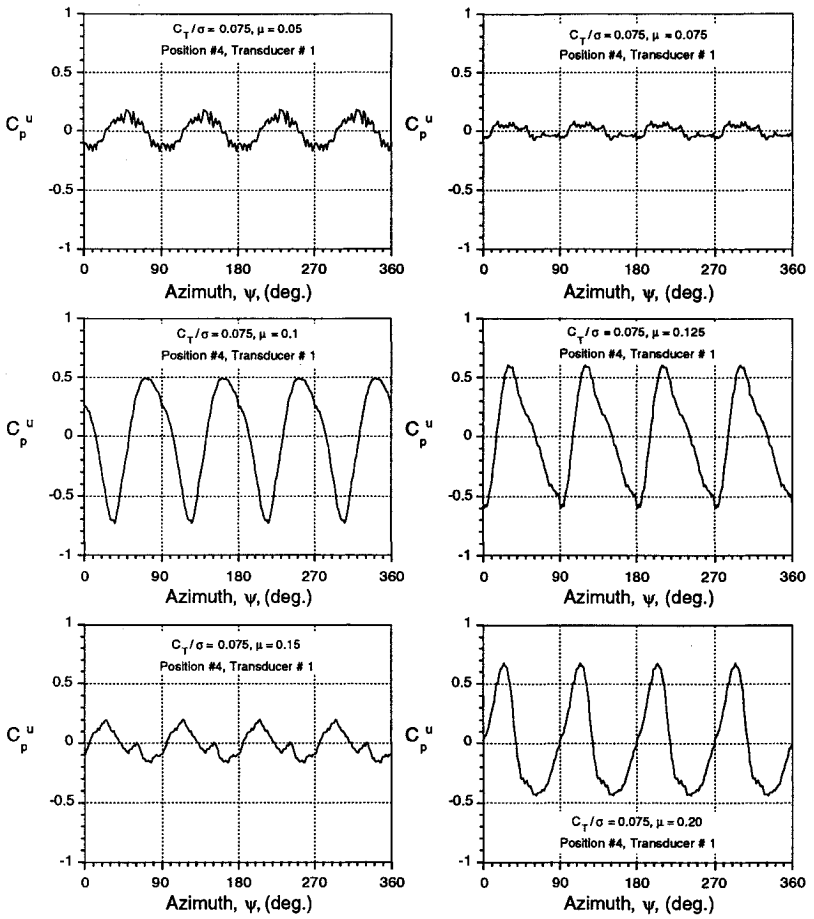

Fig. 9 Unsteady pressures measured on lifting surface as a function of advance ratio, $C_T/\sigma = 0.075$.

the leading edge (e.g., transducer no. 23, $x/c = 0.05$) to quite benign at the trailing edge (e.g., transducer no. 31, $x/c = 0.85$). It was also noticed that compared to the forward wing position there was no evidence of a blade passage-type signature measured at any point for this wing location. This is to be expected, since it is known that blade passage effects drop off very quickly away from the rotor.[13] Nevertheless, the pressure signatures measured at transducer location nos. 23 and 25 (see Fig. 8) show that strong unsteady airloads still occur.

From an examination of results at several different test points, it has been found that these complex pressure loads are related to the rotor thrust (and therefore to the strengths and convection speed of the rotor tip vortices). Furthermore, by means of the wake surveys and the shadowgraph flow visualization technique, the relative distance between the wake vortices and the measurement location were also found to be important. For example, the time-dependent pressure measured at transducer location no. 27 ($x/c = 0.385$) in Fig. 8 shows a waveform that is known to be characteristic of close (glancing) interactions of the rotor tip vortices with a surface.[31] This indicates that at this advance ratio, the rotor tip vortices were convected close to (but not necessarily impinged on) the lifting surface near transducer no. 27.

In general, the unsteady pressures measured on the upper surface of the lifting surface were found to vary significantly not only with the chordwise and spanwise location, but also with advance ratio. Figure 9 shows the effects of advance ratio on the pressure signatures measured at transducer location no. 1, which is on the upper surface at 5% chord at the 25% spanstation, i.e., the station furthest from the longitudinal centerline. This position was far enough from the rotor such that the rotor hub wake present at higher advance ratios had little effect on the measurements. While the unsteady pressures measured at advance ratios of 0.05 and 0.075 were very benign, the pressure induced at an advance ratio of 0.1 was quite significant. This is due to the fact that increasing advance ratio moves the rotor tip vortices closer to the lifting surface, and inevitably the vortices impinge on the surface at some locations. This is a strong interaction problem, most likely involving significant viscous effects.

As the advance ratio was increased from 0.1 to 0.125, the pressure signatures exhibited only relatively small changes. However, as the advance ratio was changed from 0.125 to 0.15 and then to 0.20, the magnitude of unsteady pressure response first decreased and then increased again. When the advance ratio was increased to 0.125, it was confirmed by wake studies and flow visualization that the rotor wake skew angle increased such that the most of the tip vortex filaments passed just above the top surface of the lifting surface (a glancing impingement). At an advance ratio of 0.15, the wake was skewed back so that there is less likelihood of close tip vortex/surface interactions, and the pressure responses were fairly benign. However, at an advance ratio of 0.20, the unsteady pressures were noted to increase again, even though the wake filaments were further away from the lifting surface than at $\mu = 0.15$. This is due to the unsteady noncirculatory loads induced by the higher rotor wake convection velocities and is consistent with the observations made on nonlifting bodies.[13,31] In general, the observed sensitivity of the pressure loads at different points on the wing will make the theoretical prediction of these effects a significant challenge to the analyst.

In addition, note that the time-varying downwash field induced by the convecting wake vortices must also result in local time-varying angles of attack and time-dependent circulatory loads on the wing. Therefore, there will be an unsteady wake system trailed from the wing. Besides the complexity inherent to any unsteady flow, the reduced frequencies

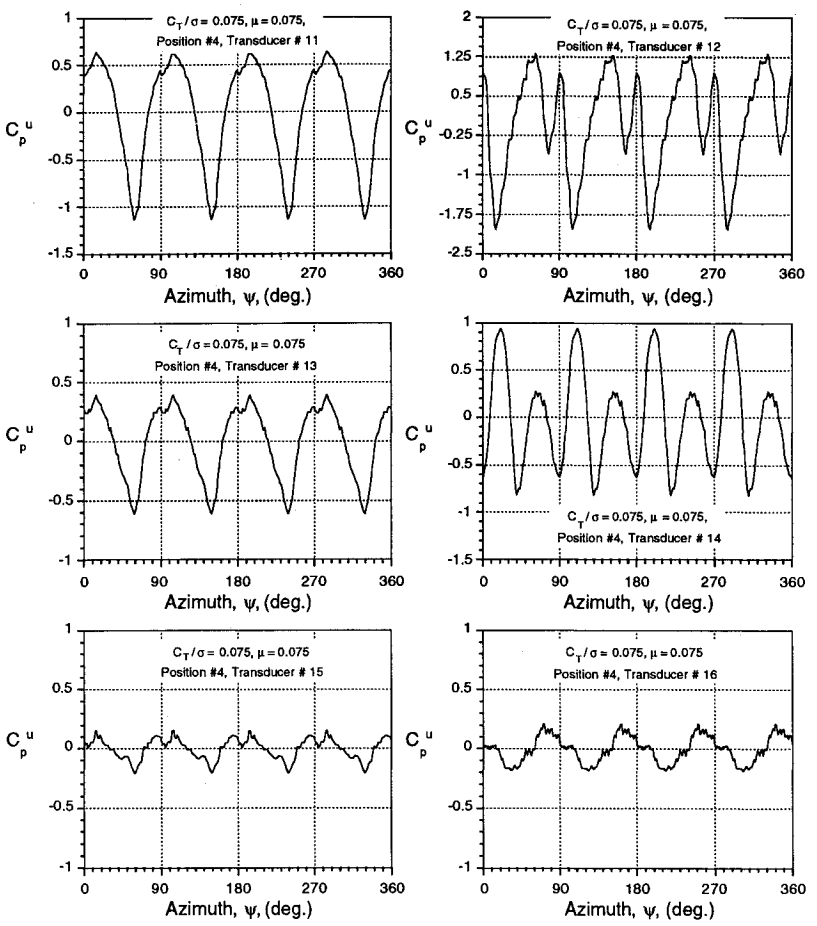

Fig. 10 Unsteady pressures measured on upper and lower surfaces at position no. 4, $C_T/\sigma = 0.075$.

($k = \omega c/2V_i$) of the rotor wake induced gust field at the lifting surface may be quite high, since

$$k = \frac{\omega c_w}{2V_i} \approx \frac{(N_b\Omega)(c_w/R)R}{2V_\infty} = \frac{N_b(c_w/R)}{2\mu}$$

The ratio c_w/R is about 0.37 for the present configuration, so that the reduced frequency of the flow at the lifting surface at an advance ratio of 0.15 would be of order 5, which is a very high value indeed. For typical helicopters, k for any empennage component will range from about 1 to 3. Clearly, this requires modeling to be considered as an unsteady problem. Also, if and when stall occurs locally on the wing, the high effective reduced frequency of the flow means that separation and stall will be dynamic in nature. This adds an additional level of complexity to the mathematical modeling of the interaction problem.

The time-dependent pressures measured on the lower surface of the lifting surface at the aft position were found to be considerably more complicated than those measured on the wing in the forward positions. Figure 10 shows a comparison between the time-dependent pressures measured on the upper and lower surfaces at transducer locations from no. 11 to no. 16 (60% spanstation). Sensor location nos. 11, 13, and 15 in Fig. 10 show that on the upper surface, the pressure signatures are representative of those that have been characterized as a close (or glancing) tip vortex/surface interaction.

However, on the lower surface, the pressures at location nos. 12 and 14 exhibit different characteristics, often with very significant double pressure peaks ($8P$). These higher harmonic pressure peaks occurred only on the lower surface of the lifting surface. The reason for this is not entirely clear. However, from examination of the flow visualization results, their existence may be related to several factors. One is the fact that some of the rotor wake vortices are massively distorted and/or perforated by the lifting surface by a cutting type of interaction.[34] Another, is that the leading edge of the rotor wake comes close to the wing position at higher advance ratios. This means that there may be two sets of trailed wake vortices convecting past the lifting surface, thus producing $8P$ contributions to the loading at some wing stations.

Summary and Conclusions

A preliminary experimental investigation has been conducted to identify the possible aerodynamic phenomena associated with the interaction of a rotor with a fixed lifting surface. The measurements suggest that the flow environment in which a lifting surface operates in a rotor flowfield is more complicated than that associated with nominally nonlifting bodies, and includes extensive regions of partial or complete flow separation and significant unsteady effects.

At low advance ratios, the rotor produces a powerful downwash that results in large negative angles of attack, and therefore separated flow on the lower surface of the wing. At higher advance ratios, the rotor induced flow becomes more streamwise resulting in a progressive transition to attached flow on the wing. In addition to these time-averaged effects, there are strong unsteady effects induced on the wing by the rotor and its wake. For wing locations below the rotor, the unsteady effects are primarily of noncirculatory origin due to $4P$ blade passage. However, for regions downstream of the rotor, the wing encounters a complex loading due to the gust field produced by the rotor tip vortices that are convected in the rotor wake. At low advance ratios, the wake slipstream is below the wing, and the unsteady airloads on the wing are benign. However, for moderately high advance ratios the rotor tip vortices are in close proximity and may impinge on the wing surface, producing $4P$ transient loads. Under some circumstances, the dominant unsteady loads are at $8P$, suggesting that both the trailing and leading edges of the rotor wake

influence the unsteady wing loading. At higher advance ratios, unsteady loads continue to build on the wing, despite the fact that the wake boundary is further from the wing surface. This is due to the higher convection velocity of the tip vortices that produce unsteady loads similar to those induced by blade passage.

Acknowledgments

This work was supported by the U.S. Army Research Office under Contract DAAL-03-88-C002 and the Minta-Martin Aeronautical Research Fund. The authors particularly wish to thank Dhananjay Samak for his contributions to this work. Thanks are due also to Olympio Mello, Terry Ghee, and Ashish Bagai for helping to build the wing model, installing instrumentation, and assisting in the tests. The Glenn L. Martin wind tunnel engineer for this test was Ahmed Kassee, and thanks are due to Jewel Barlow for his help in accommodating the tests in the wind tunnel.

References

[1]Bi, N.-P., and Leishman, J. G., "Experimental Study of Aerodynamic Interactions Between a Rotor and a Fuselage," *Journal of Aircraft*, Vol. 27, No. 9, 1990, pp. 779–788.

[2]Crouse, G. L., and Leishman, J. G., "Interactional Aerodynamic Effects on Rotor Performance in Hover and Forward Flight," *Proceedings of the 48th Annual Forum of the American Helicopter Society*, Washington, DC, 1992.

[3]Bi, N.-P., "Contributions to the Experimental Investigation of Rotor/Body Aerodynamic Interactions," Ph.D. Dissertation, Dept. of Aerospace Engineering, Univ. of Maryland, College Park, MD, May 1992.

[4]Sheridan, P. F., and Smith, R. P., "Interactional Aerodynamics—A New Challenge to Helicopter Technology," *Journal of the American Helicopter Society*, Vol. 25, No. 1, 1980, pp. 3–21.

[5]Sheehy, T. W., "A Simplified Approach to Generalized Helicopter Configuration Modeling and the Prediction of Fuselage Surface Pressures," *Journal of the American Helicopter Society*, Vol. 21, No. 1, 1976, pp. 2–8.

[6]Landgrebe, A. J., Moffitt, R. C., and Clark, D. R., "Aerodynamic Technology for Advanced Rotorcraft—Part II," *Journal of the American Helicopter Society*, Vol. 22, No. 3, 1977, pp. 2–9.

[7]Wilby, P. G., Young, C., and Grant, J., "An Investigation of the Influence of Fuselage Flow Field on Rotor Loads and the Effects of Vehicle Configuration," *Vertica*, Vol. 3, No. 2, 1979, pp. 79–94.

[8]Smith, C. A., and Betzina, M. D., "A Study of the Aerodynamic Interaction Between a Main Rotor and a Fuselage," *Proceedings of the 39th Annual Forum of the American Helicopter Society* (St. Louis, MO), American Helicopter Society, 1983.

[9]Trept, T., "A 0.15-Scale Study of Configuration Effects on the Aerodynamic Interaction Between Main Rotor and Fuselage," NASA CR 166577, Jan. 1984.

[10]Clark, D. R., and Maskew, B., "Study for Prediction of Rotor/Wake/Fuselage Interference, Part 1," NASA CR 177340, March 1985.

[11]Balch, D. T., "Experimental Study of Main Rotor/Tail Rotor/Airframe Interactions in Hover," *Journal of the American Helicopter Society*, Vol. 30, No. 2, 1985, pp. 49–56.

[12]Egolf, T. A., and Lorber, P. F., "An Unsteady Rotor/Fuselage Interaction Method," *Proceedings of the American Helicopter Society Specialist's Meeting on Aerodynamics and Aeroacoustics* (Arlington, TX), American Helicopter Society, 1987.

[13]Crouse, G. L., Leishman, J. G., and Bi, N.-P., "Theoretical and Experimental Study of Unsteady Rotor/Body Aerodynamic Interactions," *Journal of the American Helicopter Society*, Vol. 37, No. 1, 1992, pp. 55–65.

[14]Affes, H., Kim, J. M., and Komerath, N. M., "An Experimental and Analytical Study of the Interaction of a Vortex with an Airframe," AIAA Paper 92-0319, Jan. 1992.

[15]Lynn, R. R., "Lifting Surface-Rotor Interactions," *Journal of Aircraft*, Vol. 3, No. 4, 1966, pp. 326–332.

[16]Prouty, R. W., "Development of the Empennage Configuration of YAH-64 Advance Attack Helicopter," USAAVRADCOM-TR-82-D-22, Feb. 1983; also Prouty, R. W., and Amer, K. B., "The YAH-64 Empennage and Tail Rotor—A Technical History," *Proceedings of the 38th Annual Forum of the American Helicopter Society* (Anaheim, CA), American Helicopter Society, 1982.

[17]Main, B. J., and Mussi, F., "EH101—Development Status Report," *Proceedings of the 16th European Rotorcraft Forum* (Glasgow, Scotland, UK), 1990.

[18]Clark, D. R., "Analysis of the Lifting Surface/Rotor and Rotor/Rotor Interactions Present in Tilt-Rotor Aircraft," *Vertica*, Vol. 11, No. 4, 1986, pp. 731–750.

[19]McVeigh, M. A., "The V-22 Tilt Rotor Large-Scale Rotor Performance/Lifting Surface Download Test and Comparison with Theory," *Vertica*, Vol. 10, Nos. 3/4, 1986, pp. 281–298.

[20]Schillings, J. J., and Reinesch, R. J., "The Effect of Airframe Interference in V-22 Rotor Loads," *Journal of the American Helicopter Society*, Vol. 34, No. 1, 1989, pp. 26–33.

[21]McVeigh, M. A., Grauer, W. K., and Paisley, D. J., "Rotor/Airframe Interactions on Tiltrotor Aircraft," *Journal of the American Helicopter Society*, Vol. 35, No. 3, 1990, pp. 43–51.

[22]Bramwell, A. R. S., "A Theory of the Aerodynamic Interference Between a Helicopter Rotor Blade and a Fuselage and Lifting Surface in Hover and Forward Flight," Aeronautical Research Council of Great Britain, R&M 3514, June 1965.

[23]Gangwani, S. T., "A Doublet Lattice Method for the Determination of Rotor Induced Vibration Airloads—Analysis, Description, and Program Documentation," NASA CR 165893, June 1982.

[24]Gangwani, S. T., "Calculation of Rotor Wake Induced Empennage Airloads," *Journal of the American Helicopter Society*, Vol. 39, No. 2, 1983, pp. 37–46.

[25]Mello, O. A. F., and Rand, O., "Unsteady Frequency-Domain Analysis of Helicopter Non-Rotating Lifting Surfaces," *Journal of the American Helicopter Society*, Vol. 36, No. 2, 1991, pp. 70–81.

[26]Curtiss, H. C., and Quackenbush, T. R., "The Influence of the Rotor Wake on Rotorcraft Stability and Control," *Proceedings of the 15th European Rotorcraft Forum*, Amsterdam, The Netherlands, 1989.

[27]Weinstock, S., "Formulation of a Simplified Model of Rotor-Horizontal Stabilizer Interactions and Comparison with Experimental Measurements," *Proceedings of the 17th European Rotorcraft Forum* (Berlin, Germany), 1991.

[28]Leishman, J. G., and Bi, N.-P., "Investigation of Aerodynamic Interactions Between a Rotor and a Fuselage in Forward Flight," *Journal of the American Helicopter Society*, Vol. 35, No. 3, 1990, pp. 22–31.

[29]Bagai, A., and Leishman, J. G., "Experimental Study of Rotor Wake/Body Interactions in Hover," *Journal of the American Helicopter Society*, Vol. 37, No. 4, 1992, pp. 48–57.

[30]Leishman, J. G., and Bi, N.-P., "Measurements of a Rotor Flowfield and the Effects of a Fuselage in Forward Flight," *Vertica*, Vol. 14, No. 3, 1990, pp. 401–415.

[31]Bi, N.-P., and Leishman, J. G., "Analysis of Unsteady Pressures Induced on a Body by a Rotor," *Journal of Aircraft*, Vol. 28, No. 11, 1990, pp. 756–767.

[32]Howe, M. S., "On Unsteady Surface Forces, and Sound Produced by the Normal Chopping of a Rectilinear Vortex," *Journal of Fluid Mechanics*, Vol. 206, Sept. 1989, pp. 131–153.